Investigation on Effective Turbulence Models for Predicting Tanker Stern Flows

by Yusuke Tahara*, *Member* Akira Hanaoka*, *Student Member*
Koji Higaki*, *Student Member* Tomohiro Takai*, *Student Member*

Summary

This paper concerns investigation on effective turbulence models for predicting tanker stern flows. Objectives of the present work are twofold: i.e., (1) perform detailed evaluation of two equation models that are, at present, most widely accepted in numerical ship hydrodynamics; and (2) investigate feasibility in extending the models for more accurate and efficient mathematical forms. The ad-hoc approach on simple zero or one equation model is not of interest in the present work. Instead, effort will be fully focused on models that offer consistency with flow physics and possibly universal validity. The CFD code used in the present study is FLOWPACK version 2006, which was developed by the authors and its capability has been validated through detailed studies in past years. In particular, three turbulence models are investigated in the present study, i.e., the blending k-ω/k-ε model, the Shear-Stress Transport model, and the near-wall (or low-Reynolds number) modification model. In the following, an overview is given of the present numerical method, and results are presented and discussed for SR196 series tanker and KVLCC2M tanker hull forms including detailed comparisons with available experimental data. Lastly, some concluding remarks are made concerning limitations, requirements, and prognosis for improvements of the present turbulence models.

1. Introduction

As recent advancement of information technology continuously expands capability of Computational Fluid Dynamics (CFD), the Reynolds-averaged Navier-Stokes (RaNS) equation solver has matured to the point where it is widely accepted as a key tool for predicting ship boundary layer and wake flows. However, choice of appropriate turbulence model is still a point of concern, as that has been a long-lasting issue discussed in CFD workshops since 1980's [1)-5)]. The selection of sufficiently accurate mathematical model must depend on complexities of flow to be resolved. In prediction of thin boundary layer flow, the emphasis will be on relatively simple models that provide results with low computational costs; however, more complex models will be required for detailed prediction of thick boundary layer and wake flows, and/or flows with secondary swirling motion.

Closure models based on the solution of transport equations are widely accepted for industrial applications. Eddy viscosity models typically use two equations for turbulent kinetic energy k and the dissipation rate ε, or a pair of equivalent equations. Since early 1990's, simple k-ε or algebraic models have shown to be fairly satisfactory for predicting thin boundary layer flow around slender ships; however, the difficulties soon appeared in predicting tanker stern wake which involves enhanced stern bilge vortices and associated wake deformation. The above-mentioned CFD workshops were organized to identify the issue, and it finally appeared that turbulence model is the most responsible for the problem. At present, a consensus of code developers is to avoid ad-hoc approach on simple models that easily loose physical consistency, but carry out further investigation and validation of sufficiently accurate mathematical forms from high fidelity models (e.g., Reynolds-stress models) through more costless two equation models with effective corrections. Focus of the present study is more on the latter.

Objectives of the present work are twofold: i.e., (1) perform detailed evaluation of two equation models that are, at present, most widely accepted in numerical ship hydrodynamics; and (2) investigate feasibility in extending the models for more accurate and efficient mathematical forms. As claimed earlier, the ad-hoc approach on simple zero or one equation model is not of interest in the present work. Instead, effort will be fully focused on models that offer consistency with flow physics and possibly universal validity. The computational grid is generated by using the authors' in-house gridding scheme with great care for resolution and orthogonal quality. Indeed, required resolution of computational grids has been discussed through the recent CFD workshops. Especially for detailed evaluation of turbulence model, it appeared that grids in order of one million are necessary to avoid misleading conclusion due to the grid dependency of results. The CFD code used in the present study is FLOWPACK version 2006, which was developed by the authors and its capability has been validated through detailed studies in past years. In particular, three turbulence models are investigated in the present study, i.e., the blending k-ω/k-ε model[6)], the Sear-Stress Transport model[6)], and the near-wall modification

* Graduate School of Engineering, Osaka Prefecture University

Received 17th August 2007

model[7]. In the following, an overview is given of the present numerical method, and results are presented and discussed for SR196 series tanker and KVLCC2M tanker hull forms including detailed comparisons with available experimental data. Lastly, some concluding remarks are made concerning limitations, requirements, and prognosis for improvements of the present turbulence models.

2. Overview of CFD Method

FLOWPACK version 2006 is used for the flow simulation. The code has been developed by the authors, particularly for CFD education and research, and design applications for ship hydrodynamics, aerodynamics, and fluid engineering. In the transition for design applications, complete multi-block domain decomposition, automatic grid generation scheme, and CAD interface are included. At present, FLOWPACK has tight interface with both the commercial and the authors' in-house grid generators.

The numerical method of FLOWPACK solves the unsteady Reynolds-averaged Navier-Stokes and continuity equations for mean velocity and pressure. Zero or two-equation turbulence model is used for turbulent flow calculation. The equations are transformed from Cartesian coordinates in the physical domain to numerically-generated, boundary-fitted, non-orthogonal, curvilinear coordinates in the computational domain. A partial transformation is used, i.e., coordinates but not velocity components. The equations are solved using a regular grid, finite-analytic spatial and first-order backward difference temporal discretization, and PISO-type pressure algorithm. FLOWPACK is able to consider wavemaking effects by using free-surface tracking approach.

Detailed validation studies have been done for transition of the CFD method to industrial design field, through application to geometries and flows which are theoretically and/or experimentally well understood and/or well known test cases. Tahara et al.[8] concerns detailed investigation on appropriate turbulence model and near-wall flow modeling, with particular emphasis on eliminating Reynolds number (*Rn*) limitation of CFD. At present, ship full-scale flow simulation (i.e., $Rn \sim O(10^9)$) considering surface roughness effects is possible. Tahara et al.[9] is related to evaluation of accuracy in predicting ship viscous free-surface flow and propulsive performances, where self-propulsion simulation scheme was implemented into CFD. The present method was also applied to CFD-based ship-hull-form optimization, and the related documentations are available in Tahara et al.[10)-12)]. For further applications to general fluid engineering and aerodynamic designs, see Refs.[13)-15)].

3. Turbulence Models

In the following, an overview of the present turbulence model is given. In particular, three turbulence models are investigated in the present study, i.e., the blending *k-ω/k-ε* model and the Shear-Stress Transport model, both of which were originally proposed by Menter[6], and the near-wall (or low-Reynolds number) modification model proposed by Wilcox[7]. Hereafter wherever necessary, those are referred to as BSL model, SST model, and NWM model, respectively.

3.1 Blending *k-ω /k-ε* model (BSL: Baseline Model)

Perhaps, BSL model of Menter[6] is the most popular turbulence model in recent numerical ship hydrodynamics community. The basic idea of Menter is relatively straightforward, i.e., to achieve both the advantage of *k-ω* model in the sublayer and logarithmic part of boundary layers and freestream-independence of *k-ε* model in the wake region and free shear layers. A blending function F_1 is introduced, such as adding the original *k-ω* model times F_1 to *k-ε* model times $(1\text{-}F_1)$, which is transformed to *k-ω* formulation. Finally, the formulation of BSL model is given as follows,

$$\frac{Dk}{Dt} = \tau_{ij}\frac{\partial U_i}{\partial x_j} - \beta^* k\omega + \frac{\partial}{\partial x_j}\left[(\nu + \sigma_k \nu_t)\frac{\partial k}{\partial x_j}\right] \tag{1}$$

$$\frac{D\omega}{Dt} = \frac{\gamma}{\nu_t}\tau_{ij}\frac{\partial U_i}{\partial x_j} - \beta\omega^2 + \frac{\partial}{\partial x_j}\left[(\nu + \sigma_\omega \nu_t)\frac{\partial \omega}{\partial x_j}\right] + 2(1-F_1)\sigma_{\omega 2}\frac{1}{\omega}\frac{\partial k}{\partial x_j}\frac{\partial \omega}{\partial x_j} \tag{2}$$

and

$$\nu_t = \frac{k}{\omega} \tag{3}$$

where τ_{ij} is Reynolds stress tensor. The blending function F_1 is given by

$$F_1 = \tanh\left(\left\{\min\left[\max\left(\frac{\sqrt{k}}{0.09\omega\delta};\frac{500\nu}{\delta^2\omega}\right);\frac{4\sigma_{\omega 2}k}{\delta^2 CD_{k\omega}}\right]\right\}^4\right) \tag{4}$$

$$CD_{k\omega} = \max\left(2\sigma_{\omega 2}\frac{1}{\omega}\frac{\partial k}{\partial x_j}\frac{\partial \omega}{\partial x_j};10^{-20}\right) \tag{5}$$

where δ is the distance to the next surface. Let ϕ_1 represent any constant in the original *k-ω* model, ϕ_2 any constant in the transformed *k-ε* model and ϕ the corresponding constant of BSL model, then the relation between them is:

$$\phi = F_1\phi_1 + (1-F_1)\phi_2 \tag{6}$$

The sets of ϕ_1 and ϕ_2 are:

$$\phi_1 \begin{cases} \sigma_{k1} = 0.5,\ \sigma_{\omega 1} = 0.5,\ \beta_1 = 0.0750 \\ \beta^* = 0.09,\ \kappa = 0.41 \\ \gamma_1 = \beta_1/\beta^* - \sigma_{\omega 1}\kappa^2/\sqrt{\beta^*} \end{cases} \tag{7}$$

$$\phi_2 \begin{cases} \sigma_{k2} = 1.0,\ \sigma_{\omega 2} = 0.856,\ \beta_2 = 0.0828 \\ \beta^* = 0.09,\ \kappa = 0.41 \\ \gamma_2 = \beta_2/\beta^* - \sigma_{\omega 2}\kappa^2/\sqrt{\beta^*} \end{cases} \tag{8}$$

3.2 Shear-stress transport model (SST Model)

In Menter[6], the Shear-stress Transport model, i.e., SST model, is also proposed. This is a modified model of BSL, by introducing an idea to correct eddy viscosity based on Bradshaw's assumption, i.e., Reynolds stress in a boundary layer is proportional to the turbulent energy *k*. The values of ϕ_1 in SST model have to be changed so that:

$$\phi_1 \begin{cases} \sigma_{k1} = 0.85,\ \sigma_{\omega 1} = 0.5,\ \beta_1 = 0.0750 \\ \beta^* = 0.09,\ \kappa = 0.41 \\ \gamma_1 = \beta_1/\beta^* - \sigma_{\omega 1}\kappa^2/\sqrt{\beta^*} \end{cases} \tag{9}$$

$$\nu_t = \frac{a_1 k}{\max(a_1\omega; \Omega F_2)} \tag{10}$$

$$F_2 = \tanh\left(\left\{\max\left(2\frac{\sqrt{k}}{0.09\omega\delta}; \frac{500\nu}{\delta^2\omega}\right)\right\}^2\right) \tag{11}$$

where a_1=0.31 is a model constant originally used by Menter, and Ω is the absolute value of the vorticity vector. In practical applications, this model is expected to show better performance in flow with swirling motion. It is known that different values will be used for the model constant a_1 depending on condition of flows. In the present study, two values are considered for a_1, i.e., a_1=0.31 and a_1=0.155 (a half of the originally used value), and the results from these values are referred to as SST-1 and SST-2, respectively.

3.3 Near-wall modification model (NWM Model)

Wilcox[7] proposed another idea to modify the original k-ω model. It will be more universal turbulence model if both transitional regions in boundary layers and fully turbulent regions are accounted for. The Near-wall modification (NWM) model is then derived, by modifying the model constants in the original k-ω model. Turbulence Reynolds number Re_T is a key parameter in the modification. For incompressible flows, the NWM model is given by

$$\frac{Dk}{Dt} = \tau_{ij}\frac{\partial U_i}{\partial x_j} - \beta^* k\omega + \frac{\partial}{\partial x_j}\left[(\nu + \sigma^*\nu_t)\frac{\partial k}{\partial x_j}\right] \tag{12}$$

$$\frac{D\omega}{Dt} = \alpha\frac{\omega}{k}\tau_{ij}\frac{\partial U_i}{\partial x_j} - \beta\omega^2 + \frac{\partial}{\partial x_j}\left[(\nu + \sigma\nu_t)\frac{\partial \omega}{\partial x_j}\right] \tag{13}$$

and

$$\nu_t = \alpha^*\frac{k}{\omega} \tag{14}$$

The parameters α^*, α, and β^* are closure coefficients whose values are given as follows:

$$\alpha^* = \frac{\alpha_0^* + \mathrm{Re}_T/R_k}{1 + \mathrm{Re}_T/R_k} \tag{15}$$

$$\alpha = \frac{5}{9}\cdot\frac{\alpha_0 + \mathrm{Re}_T/R_\omega}{1 + \mathrm{Re}_T/R_\omega}\cdot(\alpha^*)^{-1} \tag{16}$$

$$\beta^* = \frac{9}{100}\cdot\frac{5/18 + (\mathrm{Re}_T/R_\beta)^4}{1 + (\mathrm{Re}_T/R_\beta)^4} \tag{17}$$

Subsequently, the related variables are defined by

$$\begin{cases} \beta = 3/40,\ \sigma^* = \sigma = 1/2,\ \mathrm{Re}_T = k/\omega\nu \\ \alpha_0^* = \beta/3,\ \alpha_0 = 1/10 \\ R_\beta = 8,\ R_k = 6,\ R_\omega = 2.7 \end{cases} \tag{18}$$

4. Uncertainty Assessments and Accuracy in Resistance Prediction

In use of CFD methods, uncertainty assessment must be provided for the solutions and computational grid. This is important to ensure reliability of CFD method that is used in evaluation of different turbulence models. In the following, uncertainty information of the present CFD will be given. The data are mainly from the latest work of the authors, including results from the same RaNS code and gridding method along with the similar size of computational grid as those used in the present study.

CFD uncertainty assessment consists of verification, validation, and documentation[16),17)]. Simulation uncertainty U_S is divided into two components, one from numerics U_{SN} and the other from modeling U_{SM}. The U_{SN} is estimated for both point and integral quantities and is based upon grid and iteration studies which determine grid U_G and iterative U_I uncertainties. A root sum square (RSS) approach is used to combine the components and to calculate U_{SN}, i.e., $U_{SN}^2 = U_G^2 + U_I^2$. CFD validation follows the method of Stern et al.[16)] and Wilson et al.[17)], in which a new approach is developed where uncertainties from both the simulation (U_S) and Experimental Fluid Dynamics (EFD) benchmark data (U_D) are considered. The first step is to calculate the comparison error E which is defined as the difference between the data D (benchmark) and the simulation prediction S, i.e., E=D-S. The validation uncertainty U_V is defined as the combination of U_D and the portion of the uncertainties in the CFD simulation that are due to numerics U_{SN} and which can be estimated through verification analysis, i.e., $U_V^2 = U_D^2 + U_{SN}^2$. U_V sets the level at which the validation can be achieved. The criterion for validation is that $|E|$ must be less than U_V. Note that for an analytical benchmark, U_D is zero and U_V is equal to U_{SN}. Validation is critical for making improvements and/or comparisons of different models since U_{SN} is buried in U_V.

The above-mentioned was applied to evaluate the present CFD method. Table 1 shows uncertainties and errors for total resistance for KVLCC2M towing condition (Fn=0 and Rn=3.96x10^6, where Fn and Rn are Froude number and Reynolds number based on model L_{PP} and fluid properties in experimental facility). The measured data were presented in Ref.[5)]. The size of computational grids is about one million for a half side (the starboard side). The grid uncertainty U_G is taken from the authors' previous work[9)] (where the size of computational grids is 1,250,000 and smaller grid is prepared by using refinement ratio $r = \sqrt{2}$; the order of accuracy P_G is 1.7, which is given by the previous experience, and the correction factor is given as C_G=0.8. For C_G=0.8 considered as sufficiently less than 1 and lacking confidence. For detailed definition of the variables, see Refs.[16),17)] or ITTC - Quality Manual 4.9–04–01–01[18)]). The variation in the total resistance is 0.5%D over the last period of oscillation, i.e., U_I=0.5%D. Finally, U_D=0.7%D and U_{SN}=2.06%D yield U_V=2.1%D. Four results are shown in the table, and result for SST-2 is E=–1.9%D. Hence, the CFD result for SST-2 is validated for the indicated U_V level. On the other hand, the discrepancies of frictional resistance from Schoenherr's flat plate value are within 2% for all models considered in the present study. NWM and SST-2 are around 2% lower from the Schoenherr's value, while BSL and SST-1 are 2% higher. The variation of frictional resistance is also within U_{SN}, and the similar

trend is seen for both SR196 series tanker and KVLCC2M tanker hull forms. It will be important to note that improvements of results due to different turbulence models can be considered significant if the differences are more than U_{SN} level.

Table 1: Uncertainties and errors for total resistance coefficient. KVLCC2M test case for towing condition. Fn=0 and Rn= 3.964x10^6.

Uncertainties			
U_D(%D)	U_G(%D)	U_I(%D)	U_V(%D)
0.7	2.0	0.5	2.1
Errors			
CFD(S)		EFD(D)	E(%D)
BSL	0.00439	0.00426	3.1
NWM	0.00450		5.6
SST-1	0.00444		4.2
SST-2	0.00418		-1.9

*EFD (Experimental Fluid Dynamics – Measured data)

5. Test Hull Forms and General Flow Aspects

In the present study, the computations are performed for SR196A, SR196C, and KVLCC2M tanker hull forms. SR196A and SR196C were selected hull forms in a domestic Japan joint research project SR222 (Ref.[19], unpublished). Differences between the two hulls are only on afterbody, i.e., A and C hull forms have more characterized V and U type stern framelines, respectively. Due to regulations of SR222 (SR222 non-disclosure agreements), experimental data are not directly shown in this paper; however, important flow aspects displayed in the measurements are described wherever necessary. Indeed, test cases for SR196A and SR196C hull forms are of great importance to identify trends in flow and resistance due to differences in stern form.

On the other hand, KVLCC2M tanker hull form was one of test cases at the recent CFD workshop[5]. This is a replacement of the ship models used in the earlier workshops[1)-4)], i.e., HSVA tanker and KVLCC2 tanker hull forms. Very detailed experimental data are available for public use (see Ref.[5] for more details). It is shown in the experimental data that KVLCC2M tanker hull form yields stronger stern bilge vortices than HSVA tanker hull form and the resultant deformation of axial-velocity contours is more significant. In the present study, results for KVLCC2M are used to identify accuracy of the present turbulence models through detailed qualitative and quantitative evaluation of flow and resistance.

Next, general flow features displayed in the measurements are discussed. The three tanker hull forms have similar flow patterns in the propeller plane, i.e., flow is dominated by afterbody inboard rotating bilge vortices near the centerplane, that is a common flow aspect for recent tanker hull forms. For all hull forms, so-called "hook-shaped" axial-velocity (U) contours are observed in the propeller section, which has been a challenge for CFD to accurately reproduce.

Between SR196A and C hull forms, the stern-bilge vortices are lager and stronger for the latter, and the location of vortex center for the latter is shifted outward. Consequently, the extent of "hook-shaped" U contours for SR196C is larger, which is related to the stronger stern-bilge vortices. The resultant wake distribution in propeller disk for SR196C is more uniform. This is a design concept for this hull form, i.e., more characterized U-type stern yields more uniform propeller inflow and less noise, but a drawback is more resistance.

In addition, all hull forms considered in the present study have similar Reynolds-stress field patterns. In the propeller disk area, peak value of $\sqrt{k}$ is $O(10^{-1}\ U_0)$, where U_0 is the speed of onset flow, and the extent of contours is clearly correlated with mean-flow distributions. The normal Reynolds-stresses uu, vv, and ww show similar patterns as the k values, and in fact, the turbulence is not isotropic, i.e., the axial stresses is more than twice larger than the cross plane stresses. It is also a general trend that the Reynolds stress uv is negative in region of increasing $\partial U/\partial y$, while it is positive in region of decreasing $\partial U/\partial y$ with the largest values where the gradient is the largest. The Reynolds stress uw is similar, but correlates with $\partial U/\partial z$.

6. Results and Discussion

In this section, numerical results are presented and discussed. Consider a ship fixed in the uniform onset flow $\vec{U}_\infty=(U_0,0,0)$ as depicted in Fig.1. Take the Cartesian coordinate system with the origin on the undisturbed free surface, x and y axes on the horizontal plane, and z axis directed vertically upward. In the following presentation and discussion of results, values are non-dimensionalized by using speed of onset flow U_0, fluid density ρ, and ship length L_{PP}. Note that x=0 and 1 correspond to FP and AP, respectively.

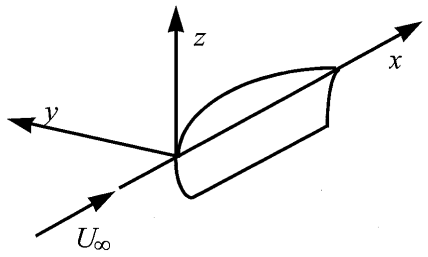

Fig.1: Definition sketch of coordinate system.

6.1 Computational grid and conditions

The volume grid is generated by using the authors' CAD-interfaced automatic gridding method. The numerical scheme is based on solutions of elliptic equations, which are solved by using exponential scheme and method of lines. An important concern for automatic gridding will be robustness to practical complexities of hull surface. Through preliminarily exercises, the present scheme was shown capable for application to modern tanker hull forms, surface combatants, and container ships, all of which are selected hull forms in the recent CFD workshops[4),5)]. In all cases, the grid orthogonality especially near the hull surface is sufficiently maintained. This gridding

scheme was also demonstrated in the authors' recent work on multi-objective optimization of a tanker hull form[10]. Fig. 2 shows an example of the grid. Overall grid topology is the O-O type, and the outer boundary is located around a ship length away from the hull surface. The grid shown in the figure includes both port and starboard sides, which enables to account for asymmetric flows due to influences of propeller action and/or drift motion. For the present study, those effects are not considered, therefore, only a half domain grid is used.

Indeed, required resolution of computational grids has been discussed through the recent CFD workshops. Especially for detailed evaluation of turbulence model, it appeared that grids in order of one million are necessary to avoid misleading conclusion due to the grid dependency of results. In the present study, the numbers of grids used are 121x100x100 (=1,210,000) in the axial, radial, and circumferential directions, respectively. The convergence criterion was that the iteration uncertainty of total resistance, defined by a half maximum amplitude in oscillation of the solution, be less than 0.5% of the averaged value, which was satisfied within 10,000 global iterations in all computations preformed in the present study.

The computational conditions basically follow those for the measurements, i.e., averaged Reynolds number Rn=4,000,000 for SR196A and C tanker hull forms, and Rn=3,945,000 for KVLCC2M tanker hull form. In addition, wave effects are assumed negligible, and the waterplane is considered to be a plane of symmetry (i.e., Fn=0 condition). As mentioned earlier, the turbulence models employed in the present computations are the blending k-ω/k-ε model, the Sear-Stress Transport model, and the near-wall modification model. Results for those are referred to as BSL, SST, and NWM results, respectively. For SST model, results for a_1=0.31 and a_1=0.155 are referred to as SST-1 and SST-2 results, respectively.

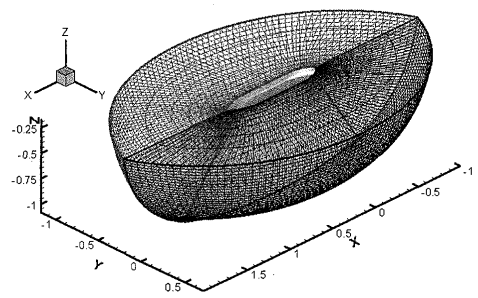

Fig.2: An example for computational grid. The topology is O-O type. In the present application, only the starboard side domain is used to simulate symmetric flow between the port and starboard sides.

6.2 Trends in flow field between SR196A and C tanker hull forms

In the following, computational results for SR196A and C tanker hull forms are discussed, with particular focus on trends in flow between the two hulls. Fig.3 shows comparison of mean-flow fields at propeller section, while Fig.4 shows comparison of normal Reynolds stress fields. It is seen that the "hook-shaped" U contours are reproduced in NWM and SST-2 results for both hulls; however, those are not seen in BSL and SST-1 results which obviously lack details. The deformation of U contours is apparently related to distribution of the V-W vectors, and the bilge vortices are predicted with larger magnitude as the "hook-shaped" U contours are more clearly reproduced.

As far as reproduction of the general flow features is concerned, NWM and SST-2 results are shown promising. The advantage of SST-2 is likely attributed to eddy viscosity correction based on Bradshaw's assumption with more correctly selected model constant a_1. It is implied that a_1=0.155 is more suitable than the originally given value, i.e., a_1=0.31, which may be due to more complexities of tanker stern flows than the flow assumed to determine the original value. As indicated in Eq.10, this model constant sets the threshold value to activate eddy viscosity correction by using the magnitude of vorticity vector, i.e., Ω. Consequently, the smaller a_1 yields the larger influences of the term related to mean-flow vorticity. At least, the present results imply a possibility to improve conventional SST model by selecting more appropriate a_1 for the present flow. In contrast, promising performance of NWL is apparently achieved by the different manner from that happens in SST-2. The possible advantages of the low-Reynolds number models for prediction of tanker stern flow were suggested by one of participants in the earlier CFD workshop[3], who applied Reynolds-stress model with low-Reynolds number corrections. Eventually, the correction yields the similar effects as those provided by SST-2; however, the authors have an impression that the effectiveness of NWM model must be supported by more validation studies, since the main advantage of this model is consideration of turbulent transitional regions in boundary layer.

On the other hand, it is noteworthy that trends in mean-flow and normal Reynolds stress fields between SR196A and SR196C hull forms are shown correct for all turbulence models applied in the present study, e.g., the stern-bilge vortices are lager and stronger for SR196C, and the location of vortex center is shifted outward. This is further confirmed by evaluation of wake coefficient (1-w_n), which is shown in Fig.5, i.e., lower values for SR196C are predicted by all models. Since extent of the above-mentioned "hook-shaped" U contours is the largest for SST-2 results, the wake coefficient for the model is the lowest for each hull form. The distributions of normal Reynolds stresses clearly correlate with the mean-flow distributions, and the contour extents are broader for SR196C than SR196A. Although it is not shown in the figure, the earlier-mentioned correlation between Reynolds stresses uv and uw with $\partial U/\partial y$ and $\partial U/\partial z$ are also confirmed for all models.

Despite several favorable results discussed above, a clear issue of the present models must be noted. That is, the anisotropic nature of normal Reynolds stresses uu, vv, and ww, are apparently missing. This is due to limitation of the underlying assumption of the present isotropic models. For more accurate prediction of mean-flow field, higher accuracy in prediction of Reynolds-stress field is undoubtedly necessary. Our future work involves challenge to the issue, e.g., it is of great interest to consider anisotropy of Reynolds-stress fields by introducing algebraic models.

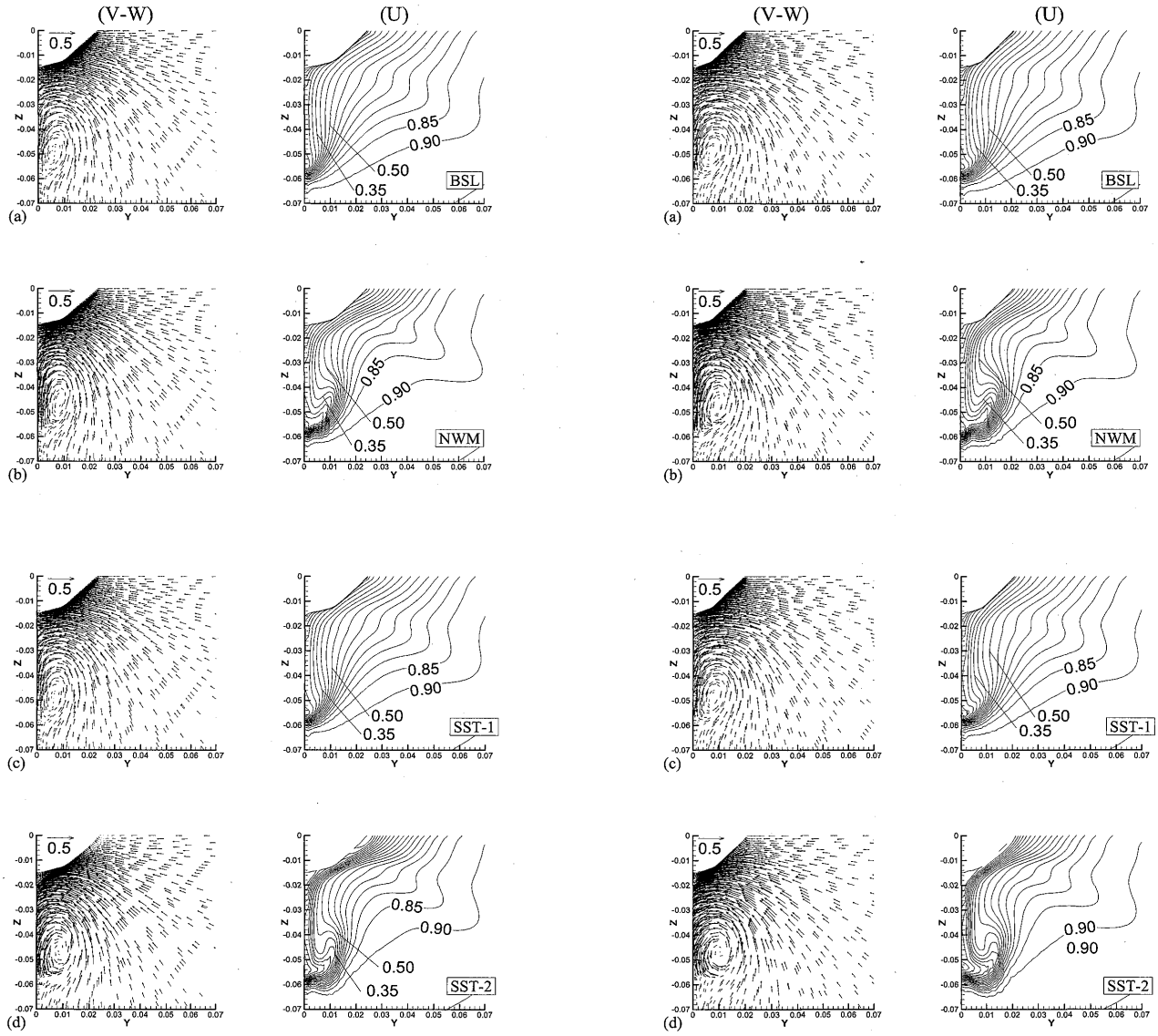

Fig.3: Comparison of solutions for SR196A and SR196C. Mean-flow fields at propeller section (X=0.988). Rows, (a) BSL, (b) NWM, (c) SST-1, and (d) SST-2.

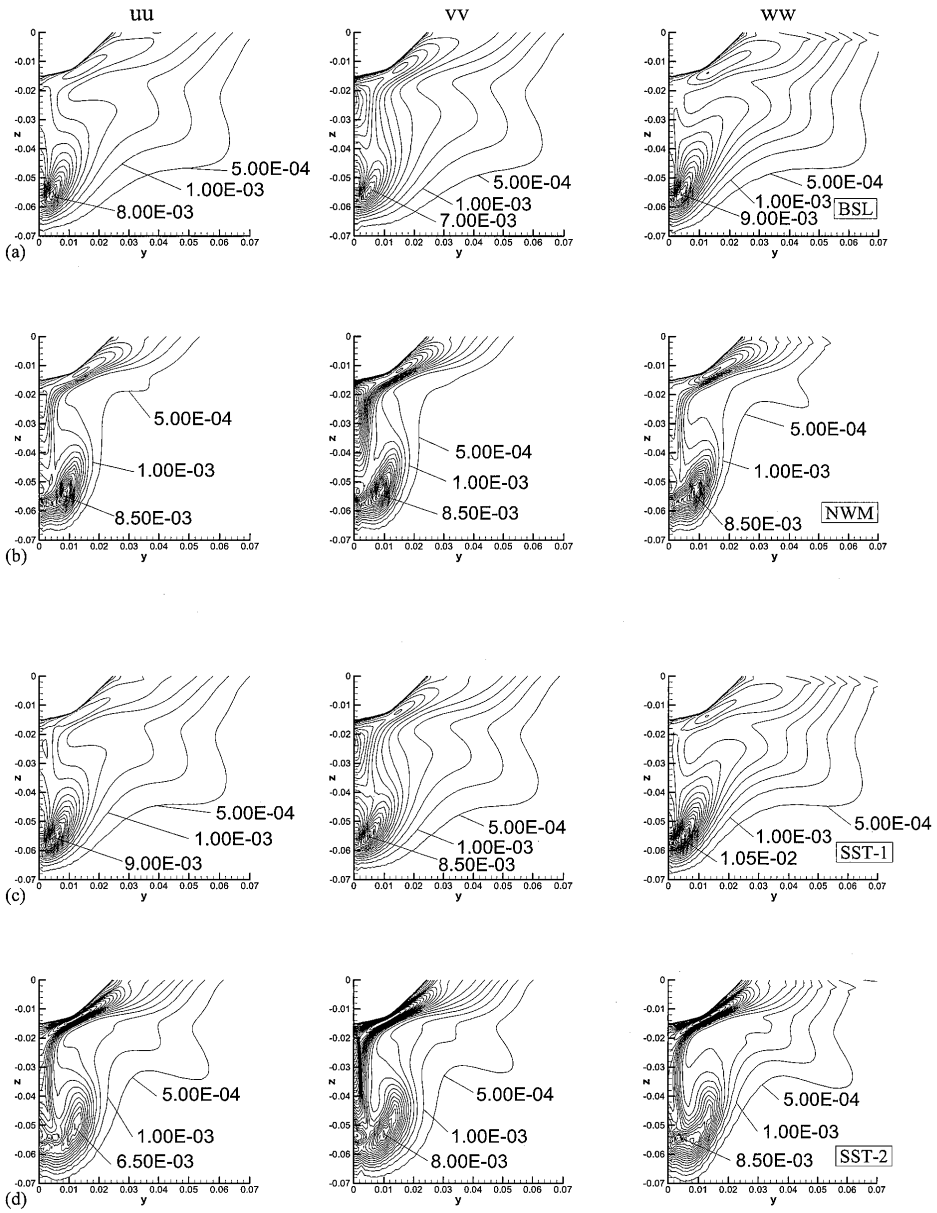

Fig.4: Comparison of solutions for SR196A. Reynolds-stress fields at propeller section (X=0.988). Rows, (a) BSL, (b) NWM, (c) SST-1, and (d) SST-2.

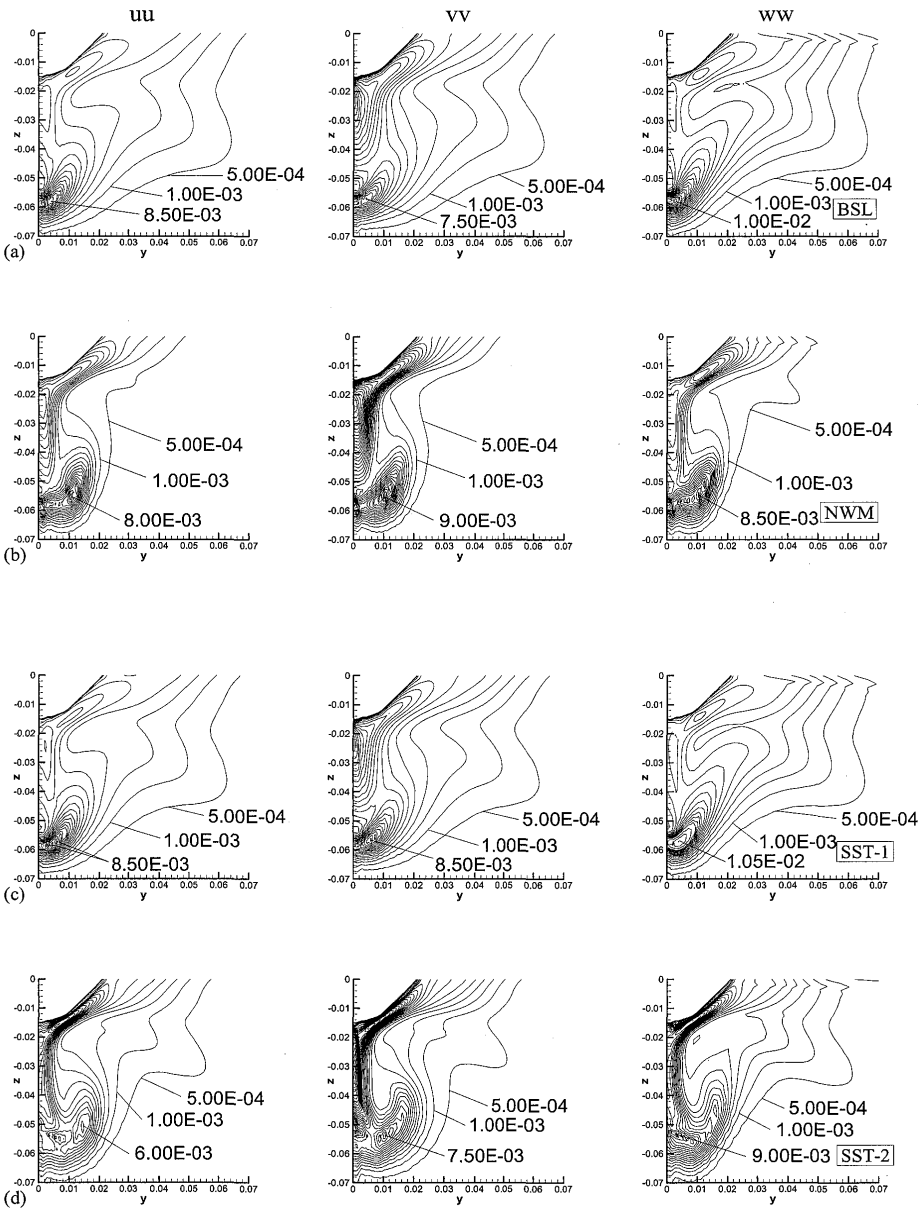

Fig.4 - Continued. For SR196C.

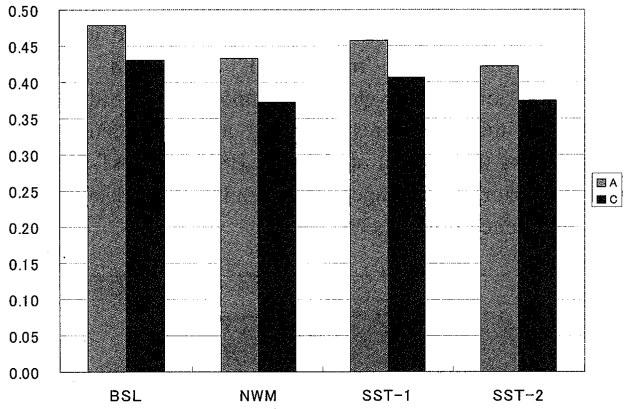

Fig.5: Comparison of wake coefficient (1-w_n) between SR196A and C tanker hull forms.

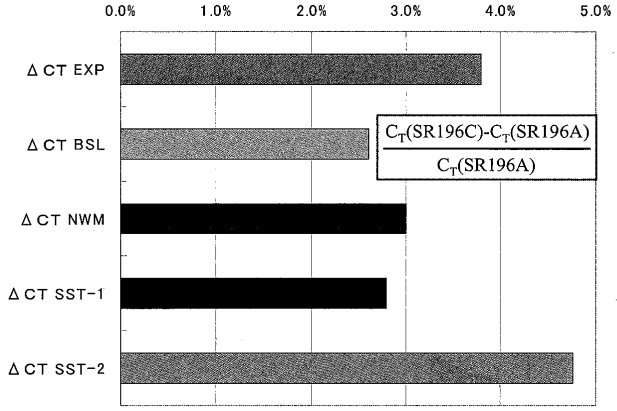

Fig.6: Comparison of trends in total resistance between SR196A and C tanker hull forms.

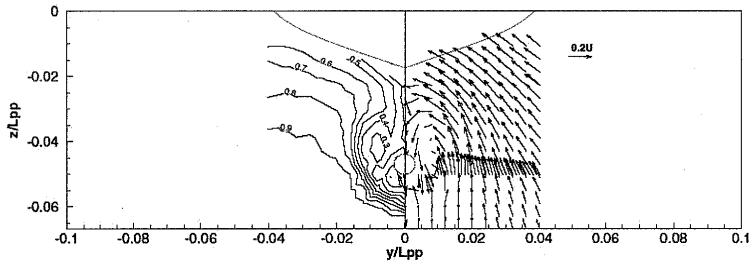

(a) EXP.

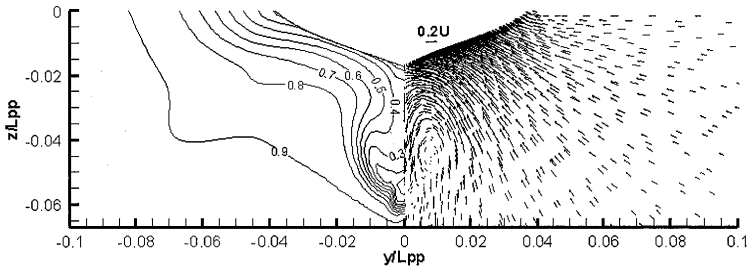

(b) NWM

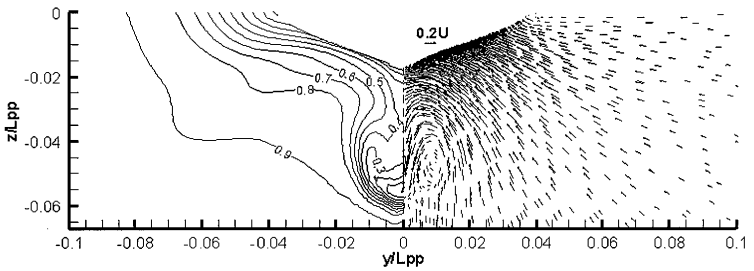

(c) SST-2

Fig.7: Comparison of U contours and V-W vectors at propeller section for KVLCC2M tanker hull form. Rows, (a) Experiments, (b) NWM, and (c) SST-2.

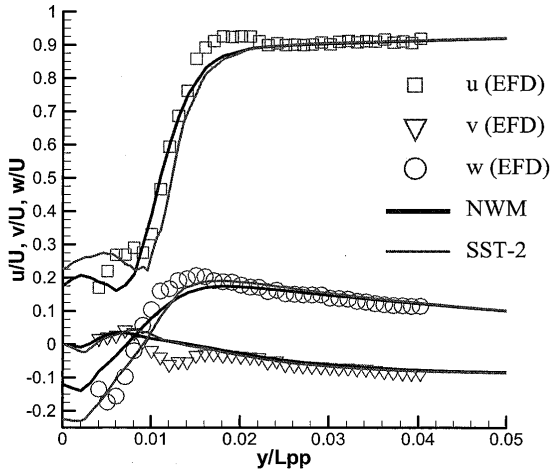

Fig.8: Comparison of velocity profiles along Z=−0.05 line (near the center of propeller shaft) at propeller section for KVLCC2M tanker hull form.

6.2 Trends in resistance between SR196A and C tanker hull forms

Integration of surface pressure and shear-stress distributions over the hull surface yields the pressure and frictional resistances, respectively, and the sum is total resistance. Fig.6 shows comparison of the values, where the values are plotted in relative % to that for SR196A to display trends in resistance. The trend between A and C hull forms in the measurement is correctly reproduced by all three models, i.e., total resistance of SR196C hull form is larger than that of SR196A hull form. The differences in total resistance between the two hull forms are mainly due to differences in pressure resistance. Regarding the magnitude, SST-2 and others over and under predict the experimental value, respectively; however in fact, the discrepancies from experimental value can be considered within the range of simulation uncertainties U_{SN} for all models.

6.3 Flow and resistance for KVLCC2M tanker hull form

In the following, more detailed evaluation of the present turbulence models is discussed through comparison of results for KVLCC2M tanker hull form. For this hull form, presentation of detailed experimental data is possible.

First, comparison of mean-flow field at propeller section is discussed. Fig.7 shows comparison of U contours and V-W vectors at the propeller section, where results for NWM and SST-2 are presented. In addition, Fig.8 shows comparison of velocity profiles along Z=−0.05 line (near the center of propeller shaft) at the same station. It is seen that gross features of flow displayed in the measurements are well predicted in the two computational results, i.e., the strength and location of stern-bilge vortices and associated deformation of axial-velocity contours ("hook-shaped" U contours) are well reproduced.

It is shown that SST-2 results are in somewhat closer agreement with the measurements regarding distribution of velocity near the centerplane, e.g., shapes of U=0.3 and 0.4 contours are more similar to those displayed in the measurements (Fig.7). This is consistent with the velocity profiles (Fig.8), i.e., slightly better agreement with the measurements is achieved in SST-2 results especially near the centerplane (i.e., Y=0). The differences between the two models are apparently related to accuracy in reproducing secondary motion of flow and associated deceleration of axial velocity component. Although not included in the figure, results from other turbulence models considered in the present study, i.e., BSL and SST-1, indicate clearly inferior performance and results lack details of the above-mentioned flow aspects.

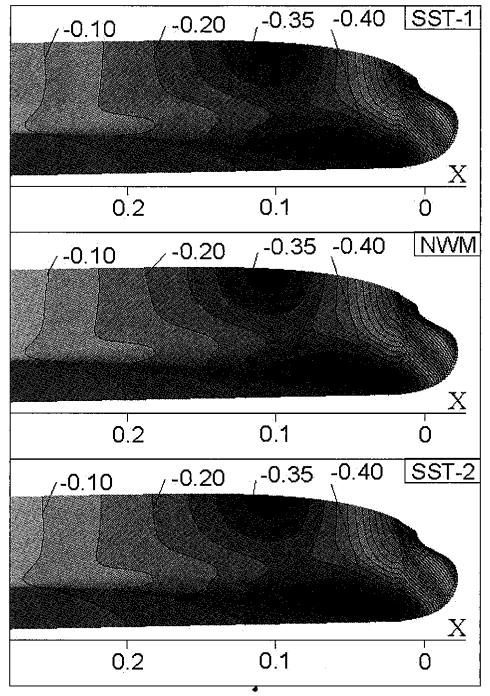

(a) Near bow region

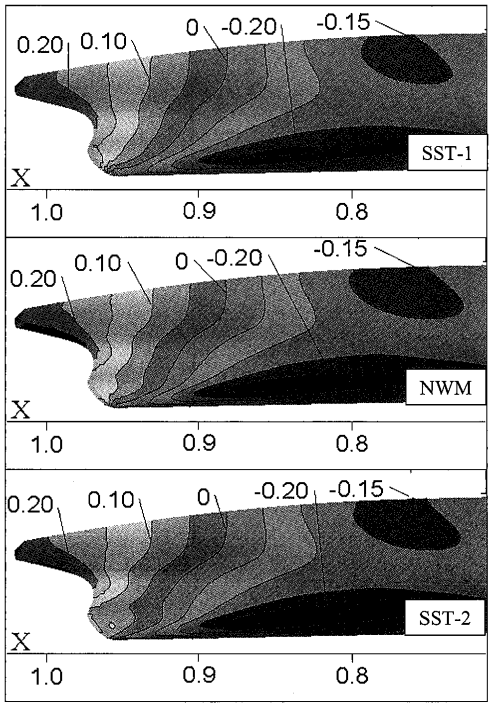

(b) Near stern region

Fig.9: Comparison of surface pressure contours for KVLCC2M tanker hull form. (a) and (b) shows near bow and stern regions, respectively.

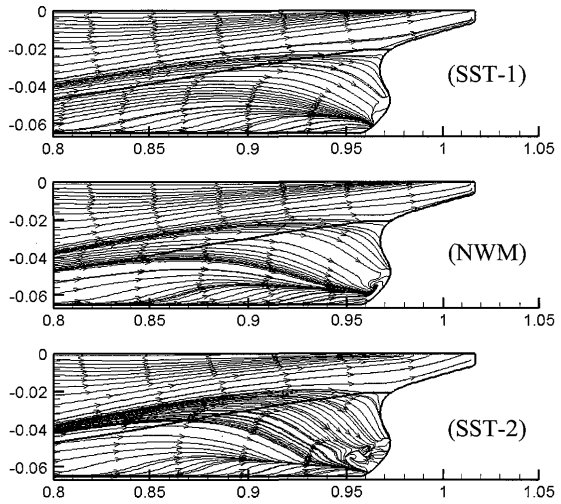

Fig.10: Comparison of frictional streamlines for KVLCC2M tanker hull form.

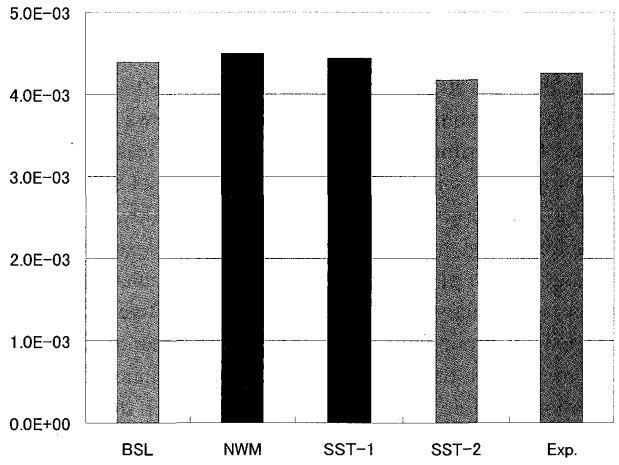

Fig.11: Comparison of total resistance coefficient for KVLCC2M tanker hull form.

Next, surface pressure and near-wall flow fields are discussed. Figs.9 and 10 show comparison of surface pressure contours and frictional streamlines, where in addition to NWM and SST-2 results, SST-1 results are also included in order to identify relative shortcomings in comparison to others. As described below, the general features of surface pressure and associated near-wall flows for the present hull form are commonly seen for recent tanker hull forms (e.g., see Ref.[4),5)]). On the forebody, a pressure pocket (low pressure region) exists near the bilge, which causes the streamlines towards the keel. On the midbody, streamwise pressure distribution is relatively flat and the streamlines are mostly parallel, which is due to the parallel part often designed for the modern tanker hull forms. On the afterbody, a pressure pocket is located near the stern bilge, which causes the streamlines to converge towards the stern bilge, and the streamlines meet those from the flat bottom and finally form the stern-bilge vortices. The above-mentioned flow features are well predicted in the present computations.

On the other hand, differences in surface pressure contours among the three turbulence models are highlighted near the stern, which correlates with the significant differences in streamlines. The differences are especially obvious in the region near the stern bilge, i.e., extent and depth of the pressure pocket differ among the models. The pressure pocket is broader and deeper for NWM and SST-2 results than SST-1 results, and the influences on the streamlines appear very significant. Convergence of streamlines occurs in the region is directly related to generation of stern-bilge vortices, which is apparently with smaller scale for SST-1. This results in the larger and stronger stern-bilge vortices predicted in the NWM and SST-2 results. Between the NWM and SST-2 results, differences in surface pressure and frictional streamlines are seen near the stern bulb, where more complexities especially for the streamlines are observed in SST-2 results. The separation pattern displayed in the local region apparently has significant influences on the near wake and the details must correctly be predicted.

Finally, accuracy in predicted total resistance is discussed. Fig.11 shows comparison of the values, where results for all turbulence modes considered in the present study are included. For all turbulence models, discrepancies from EFD result are within 5%D (D: EFD result), and it appears that SST-2 result is the closest to EFD result and the error E is –1.9%D. In authors' judgment, the agreement between CFD and EFD results is satisfactory for this level of grid size, which is based on a fact that in other results presented in the recent CFD workshop[5)] for the same ship model and test condition (12 participants used RaNS code), E varies from –9.3%D through 8.8%D and the averaged $|E|$ is 5.1%D.

7. Concluding Remarks

This paper concerns investigation on effective turbulence models for predicting tanker stern flows. Objectives are twofold: i.e., (1) perform detailed evaluation of two equation models that are, at present, most widely accepted in numerical ship hydrodynamics; and (2) investigate feasibility in extending the models for more accurate and efficient mathematical forms. In particular, three turbulence models were investigated in the present study, i.e., the blending k-ω/k-ε model (BSL), the Shear-Stress Transport model (SST), and the near-wall modification model (NWM). For SST model, two model constants are considered and results are compared, i.e., SST-1 and SST-2. An overview was given of the present numerical method, and results were presented and discussed for SR196A and C, and KVLCC2M tanker hull forms including detailed comparisons with available experimental data. In the present study, results for SR196 series tanker hull forms were used to identify accuracy of the present turbulence models in predicting trends in flow and resistance due to differences in stern form, while results for KVLCC2M tanker hull form were used for more detailed qualitative and quantitative evaluation of the results.

It is shown in the present results that trends in flow and resistance between SR196A and C tanker hull forms are correctly predicted by all turbulence models considered in the present study; however, NWM and SST-2 models indicate very promising performance in detailed prediction of flows. The

advantage of SST-2 model is likely attributed to eddy viscosity correction based on Bradshaw's assumption with more correctly selected model constant a_1. It is implied that a_1=0.155 is more suitable than the originally given value, i.e., a_1=0.31, which may be due to more complexities of tanker stern flows than the flow assumed to determine the original value. At least, the present results imply a possibility to improve conventional SST model by selecting more appropriate a_1 for the present flow. Promising results for NWM model are rather unexpected since the main advantage of this model is consideration of turbulent transitional regions in boundary layer, therefore, the effectiveness must be supported by more validation studies. In order to ensure the above-mentioned, the present study will be continued through the application to more complex flows, e.g., tanker stern flows for drift condition for which very detailed experimental data are available[5].

Our future work will also involve extension of the present models for more accurate and efficient mathematical forms. As already stated, the lack of anisotropic nature of the normal Reynolds-stress fields is a clear issue found through the present study. For more accurate prediction of mean-flow field, higher accuracy in prediction of Reynolds-stress field is undoubtedly necessary. For example, it is of great interest to consider anisotropy of Reynolds-stress fields by introducing algebraic models. Some of the above-mentioned future work are already in progress, and will be reported in future publications.

Acknowledgements

The present work has been partly supported by Grant-in-Aid for Scientific Research, Japan (2002-2005, Project Number 14350524; and 2006-2008, Project Number 18360422), and the Office of Naval Research (2002-2005, Grant Number N00014-05-1-0616; and 2005-2008, Grant Number N00014-02-1-0304) under the administration of Dr. P. Purtell and Dr. H. Narita. The authors wish to express their appreciation to those who concern the program for their kind support and encouragement.

Reference

1) Larsson, L (Ed.) 1981. SSPA-ITTC workshop on ship boundary layers. SSPA Report, No.90, SSPA Publication, Gothenburg, Sweden
2) Larsson, L., Patel, VC, Dyne, G. (Eds.) 1991. Flowtech Research Report, No.2, Flowtech International, Gothenburg, Sweden
3) Kodama, Y. (Ed.) 1994. CFD Workshop Tokyo. Ship Research Institute, Ministry of Transport and Ship & Ocean Foundation, 22-24 March, Tokyo, Japan, Vol.1 and 2
4) Larsson, L, Stern, F, Bertram, V. 2000. Summary conclusions and recommendations of the Gothenburg 2000 workshop. Gothenburg 2000: A Workshop on Numerical Ship Hydrodynamics, September, Chalmers University of Technology, Gothenburg, Sweden
5) Hino T (Ed.) 2005. CFD Workshop Tokyo 2005. National Maritime Research Institute, 9-11 March, Tokyo, Japan
6) Menter, F.R. 1994. Two-Equation Eddy- Viscosity Turbulence Models for Engineering Applications. AIAA Journal. 32(8): 1598- 1605
7) Wilcox, D.C. 1994. Simulation of Transition with a Two-Equation Turbulence Model. AIAA Journal. 32(2): 247-255
8) Tahara, Y., Katsui, T., Himeno, Y. 2002. Computation of Ship Viscous Flow at Full Scale Reynolds Number - Consideration of Near-Wall Flow Model Including Surface Roughness Effects. J. Society of Naval Architects of Japan 192:89-101
9) Tahara, Y., Wilson, R., Carrica, P., Stern, F. 2006. RANS Simulation of a Container Ship Using a Single-Phase Level Set Method with Overset Grids and Prognosis for Extension to Self-Propulsion Simulator. J. Marine Science and Technology 11(4):209-228
10) Tahara, Y., Tohyama, S., Katsui, T. 2006. CFD-Based Multi-Objective Optimization Method for Ship Design. International J. Numerical Methods in Fluids 52:449-527
11) Campana, E.F., Peri, D., Tahara, Y., Stern, F. 2006. Shape Optimization in Ship Hydrodynamics Using Computational Fluid Dynamics. J. Computer Methods in Applied Mechanics and Engineering 196: 634–651
12) Tahara, Y., Stern, F., Himeno, Y. 2004. Computational Fluid Dynamics-Based Optimization of a Surface Combatant. J. Ship Research 48(4): 273-287
13) Tahara, Y., Hayashi, G. 2003. Flow Analyses around Downwind-Sail System of an IACC Sailing Boat by a Multi-Block NS/RaNS Method. J. Society of Naval Architects of Japan 194:1-12
14) Tahara, Y. 2006. Development and Demonstration of Simulation Based Design for Parachute Aerodynamic Design. 7th International Conference on Hydrodynamics, Ischia, Italy: 511-518
15) Tahara, Y., Katsui, T., Himeno, Y. 2004. Development of Simulation Based Design for Ship Hydrodynamics and Fluid Engineering. 4th Conference for New Ship & Marine Technology, Shanghai : 1-13
16) Stern F., Wilson R.V., Coleman H.W., Paterson E.G. 2001. Comprehensive Approach to Verification and Validation of CFD Simulations - Part 1: Methodology and Procedures. J. Fluids Eng. 123: 793-802
17) Wilson R.V., Stern F., Coleman H.W., Paterson E.G. 2001. Comprehensive Approach to Verification and Validation of CFD Simulations - Part 2: Application for RANS Simulation of a Cargo/Container Ship. J. Fluids Eng. 123: 803-810
18) ITTC - Quality Manual (4.9–04–01–01). 2002. 23rd International Towing Tank Conference, Venice, Italy
19) SR222 Final Report. 1996. Shipbuilding Research Association of Japan, [Japanese, unpublished]